Gutsche, C. S.; Gräfe, S.; Gitter, B.; Flanagan, K. J.; Senge, M. O.; Kulak, N.; Wiehe, A. (2018):
Pre-/post-functionalization in dipyrrin metal complexes – antitumor and antibacterial activity of their glycosylated derivatives.
Dalton Transactions 47, 12373–12384. doi: 10.1039/C8DT03059F

Journal Name

ARTICLE

Pre- and Post-functionalization in Dipyrrin Metal Complexes – Antitumor and Antibacterial Activity of Glycosylated Gallium Complexes

Received 00th January 20xx,
Accepted 00th January 20xx

DOI: 10.1039/x0xx00000x

www.rsc.org/

Claudia S. Gutsche,[a,b,c] Susanna Gräfe,[c] Burkhard Gitter,[c] Keith J. Flanagan,[d] Mathias O. Senge,[d] Nora Kulak[a] and Arno Wiehe*[b,c]

A post-functionalization route to tris(dipyrrinato) metal complexes is presented giving access to a range of new complexes relevant in the context of medicinal inorganic chemistry. A pentafluorophenyl group in the meso-position of the dipyrrin ligand serves as an anchor for the connection with alcohols and thiocarbohydrates. The photochemotherapeutic activity of the complexes has been assessed in cellular assays with tumor cell lines and against the Gram-positive bacterium *S. aureus*. Finally, it is shown that this post-functionalization is also applicable to other dipyrrinato metal complexes.

Introduction

The introduction of metal-based drugs has proven to be useful for diverse therapeutic and diagnostic purposes.[1] Hence, medicinal inorganic chemistry allows for the development of drugs with new mechanisms of action.[1c,2] The most prominent metal complex is cisplatin, which has initiated the field of medicinal inorganic chemistry.[1e,3] Despite its widespread clinical use as a chemotherapeutic agent there is a need for the development of new and improved anticancer drugs due to several drawbacks of cisplatin.[3e,h] Metal complexes containing ruthenium[1f,4] and gallium[1f,4a,5] have shown promising properties in this respect.

Dipyrrins,[6] also known as dipyrromethenes, can serve as ligands in bis(dipyrrinato)[6,7] or tris(dipyrrinato) complexes.[6,7a,b,8] Dipyrrins become more stable when substituted with electron-withdrawing groups and conformationally more flexible when unsubstituted in the α-position.[6,7b,c] Complexes with dipyrrin ligands have, up to now, found mostly applications in material sciences.[8e,f,g,9] An application in the biomedical arena requires the balance of hydrophobic and hydrophilic properties of the compounds, as well as the substitution with moieties facilitating cell uptake like carbohydrates.[10] Usually, functionalized dipyrrinato metal complexes are synthesized by preparing the functionalized ligand and then forming the metal complex in the final step.[11] However, labile functional groups are sometimes incompatible with this strategy. Hence, methods for introducing substituents into the assembled complex are of specific interest.[11b]

Herein, a post-functionalization route to tris(dipyrrinato) metal complexes of iron, indium, and gallium is presented. The synthesis makes use of the nucleophilic substitution (S_NAr) on the *meso*-pentafluorophenyl (PFP) moieties of the dipyrrin ligands. This nucleophilic substitution in the *para*-position of the PFP substituents has already proven to be a valuable tool for the functionalization of diverse porphyrinoids.[10e,12] Alternatively, the application of pre-functionalized dipyrrins as ligands for the synthesis of these tris(dipyrrinato) complexes is exemplified. The phototoxicity of selected complexes was evaluated in cellular assays with several tumor cell lines and against the Gram-positive bacterium *S. aureus*.

Furthermore, it is shown that this post-functionalization approach is also applicable to other metal complexes by transferring the reaction conditions to the reaction of PFP-substituted (dipyrrinato)bis(bipyridyl) ruthenium(II) complexes with nucleophiles.

Additionally, in this publication the structures of five new tris(dipyrrinato) metal(III) complexes, with either indium(III), gallium(III), or iron(III) centers, are described. The structural elucidation of tris(dipyrrinato)metal complexes was first reported in 1997 by Brückner *et al*. and over the following decades, several such structures have been deposited to the Cambridge Crystallographic Data Center (CCDC) database.[8i]

[a] *Institut für Chemie und Biochemie, Freie Universität Berlin, Fabeckstr. 34/36, 14195 Berlin, Germany.*
[b] *Institut für Chemie und Biochemie, Freie Universität Berlin, Takustr. 3, 14195 Berlin, Germany.*
[c] *biolitec research GmbH, Otto-Schott-Str. 15, 07745 Jena, Germany, e-mail: arno.wiehe@biolitec.de.*
[d] *Medicinal Chemistry, Trinity Translational Medicine Institute, Trinity Centre for Health Sciences, Trinity College Dublin, The University of Dublin, St. James's Hospital,Dublin 8, Ireland..*

Electronic Supplementary Information (ESI) available: [details of any supplementary information available should be included here]. See DOI: 10.1039/x0xx00000x

CCDC 1841032–1841036 contain the supplementary crystallographic data for this paper. These data can be obtained free of charge from The Cambridge Crystallographic Data Centre via www.ccdc.cam.ac.uk/data_request/cif.

These compounds have found a variety of uses over the years with one of the main features being its incorporation into metal–organic frameworks and non-covalent networks.[X1] This is due to their characteristic octahedral shape that the tris(dipyrrinato) motifs form around their metal(III) centers, the planar conformation of the dipyrrin ligand, and a variety of short contacts that can be achieved due to various substitutes on the dipyrrin ligand. These features typically generate an appealing packing pattern for metal–organic frameworks or host–guest complexes. For the compounds studied herein, these characteristics will be the focus of the discussion, as well as how the presentation of fluorine atoms on the aromatic rings adds a unique element to the packing pattern of tris(dipyrrinato)metal complexes, which to date, has not been studied.

Results and discussion

The reaction of purified and isolated PFP-dipyrrin[7c] **1** with $InCl_3$, $GaCl_3$, or $FeCl_3{\cdot}6H_2O$, respectively, in the presence of a base (DIPEA), gave complexes **2**-**4** (Scheme 1). Complex **4** has previously been described in the literature.[7b]

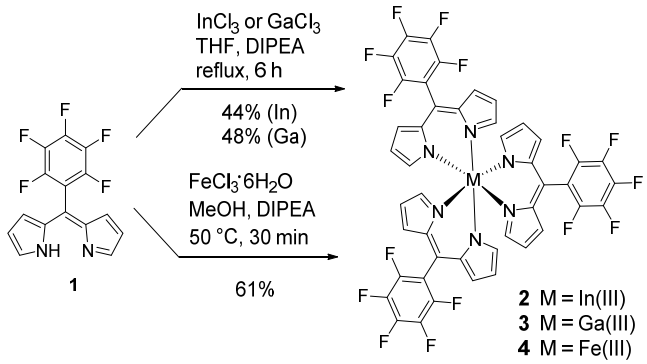

Scheme 1 Synthesis of tris(dipyrrinato) metal complexes **2**-**4**.

In Figure 1 the absorption spectra of dipyrrin **1** and the complexes **2**-**4** are shown.

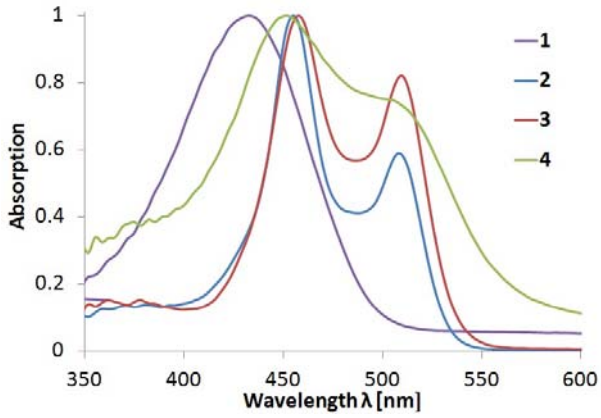

Figure 1. Absorption spectra (normalized) of dipyrrin **1** and tris(dipyrriato) metal complexes **2**-**4** in DCM.

As can be seen, the absorption spectra of the three tris(dipyrrinato) metal complexes (Figure 1) show two pronounced absorption bands at ~450 and ~515 nm. This differs significantly from the single broad absorption band of dipyrrin ligand. The absorption spectra of the gallium(III) and indium(III) complex are very similar whereas the spectrum of the iron(III) complex is considerably broadened.

Crystals suitable for X-ray structural characterization were obtained for compounds **2** and **3** (Figures 2 and 3). Their structures are the first of examples of tris(dipyrrinato)metal complexes bearing a pentafluorophenyl (PFP) unit on the meso-position. These two structures have two separate packing patterns, however, both structures feature several F···H contacts, which appear to be directional within each respective structure. The packing of compound **2** and **3** is likely to be influenced by the metal(III) center due to N–M bond lengths, adding to the distinction of their packing patterns. Both compounds **2** and **3** crystallized with one complete molecule in the asymmetric unit. For simplicity, the dipyrrin units surrounding the metal(III) centers in the structures have been labelled A, B, and C following the atom label, as seen in Figures 2 and 3.

The structure of compound **2** has a bifurcated interaction centered on the proton of C1B. These are C1B–H1B···F2B [2.615(1) Å, 117.2(1)°] and C1B–H1B···F4A [2.615(1) Å, 114.3(1)°], which forms a head-to-head H···F network of interactions. Additionally, there is a H···F interaction between C3A–H3A···F3B [2.519(1) Å, 162.9(1)°], which forms a zig-zag network within the crystal structure. Other interactions of note are C2A–H2A···F3A [2.525(1) Å, 147.3(1)°] and the reciprocal dimer interaction of F1B···F2B [2.837(2) Å]. This forms the rather complex packing pattern seen in Figure S 1. There is an almost octahedral orientation of ligands around the metal(III) center with an N–In–N angle range of 84.6(5)–95.2(5)° and an N–In bond length range of 2.188(1)–2.243(1) Å. Additionally, there is an In···In distance of 8.402(1)–9.347(1) Å to the nearest neighboring molecule. Interestingly, it appears that the C-subunit in this structure forms no apparent interactions or short contacts.

In compound **3**, the F···H interactions observed are much simpler than those of **2**. The F···H contacts of C7A–H7A···F1A [2.458(2) Å, 173.0(2)°] and C7B–H7B···F5B [2.435(2) Å, 141.9(2)°] are repeated between all units, holding the structure at a Ga···Ga distance of 8.837(1)–8.904(1) Å to the nearest neighboring molecule. This is clearly represented in the moiety packing of compound **3** (Fig. S 2). Additionally, the N–Ga–N angle range of 88.3(1)–92.6(1)° and an N–Ga bond length range of 2.046(3)–2.084(3) Å forms an octahedral complex around the Ga(III) metal center.

There are only minor differences between compounds **2** and **3** due to the metal(III) centers, which results in compound **2** having a longer N–M bond length between the ligand and metal(III) center and a larger N–M–N angle. Aside from this, both structures result in an octahedral complex. This difference appears to impact the potential F···H networks formed in both samples, with compound **2** containing many more short contacts compared to compound **3**.

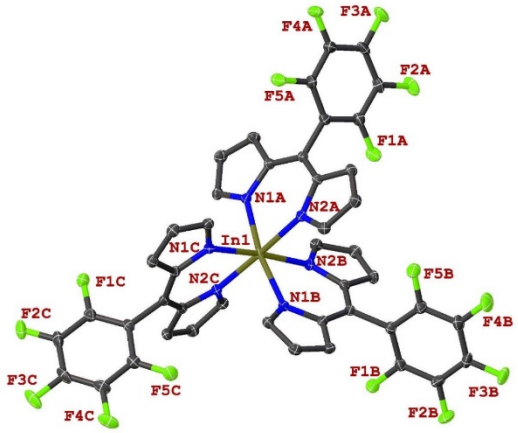

Figure 2. View of the molecular structure of complex **2** in the crystal. Hydrogen atoms and labels for carbon atoms have been omitted. Thermal ellipsoids give 50% probability.

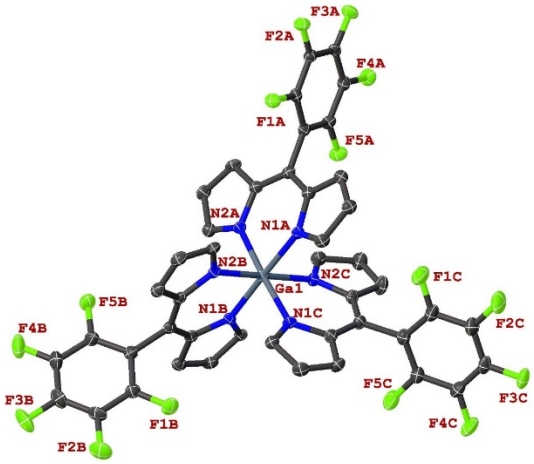

Figure 3. View of the molecular structure of complex **3** in the crystal. Hydrogen atoms and labels for carbon atoms have been omitted. Thermal ellipsoids give 50% probability.

As a test reaction, complex **3** was reacted with selected alcohols under reaction conditions typical for nucleophilic substitution on the PFP moiety (alcohol in excess, solid KOH, Scheme 2).[10e,13] In all cases, the substituted complexes **5a**-**c** were obtained in moderate yields.

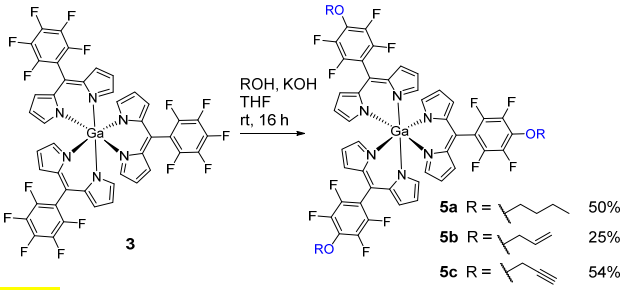

Scheme 2 Substitution reaction of **3** with alcohols.

The absorption spectra of these complexes **5a**-**c** (Fig. 4) show no pronounced differences compared to the non-functionalized complexes **2**-**4**. This is not unexpected as the phenyl ring carrying the substituent is twisted to the plane of the dipyrrin (see below and above the X-ray structures of complexes **2** and **3**) by 90–100° for compound **2** and 73–94° for compound **3**. Therefore, the substituent has only a very limited influence on the electronic structure of the dipyrrin unit.

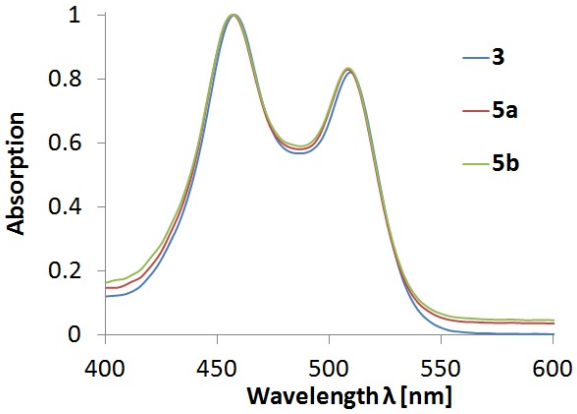

Figure 4. Absorption spectra (normalized) of tris(dipyrriato) gallium complex **3** and the alkoxy-substituted gallium complexes **5a**,**b** in DCM.

Crystals suitable for X-ray structural characterization were obtained for compound **5a** (Fig. 5). The structure of **5a** solved with only a 1/3 of the molecule present in the asymmetric unit. This structure differs from compound **3** due to the now substituted 4-position, which contains a butyloxy group. This alternate substitution has quite an impact on the F···H networks formed and results in an artistic kaleidoscope–type pattern of packing in the unit cell (Fig. 5a). The structure of **5a** shows two major F···H contacts, C17–H17A···F3 [2.405(1) Å, 158.2(1)°] and C6–H6···F1 [2.406(1) Å, 157.8(1)°]. However, due to the high symmetry within this structure, these interactions are repeated three times in one unit creating an elaborate F···H network within the structure. This results in a shorter Ga···Ga distance of 7.595(1) Å to the nearest neighboring molecule, as compared to compound **3**. The N–Ga–N angle range of 88.3(1)–90.6(1)° and an N–Ga bond length range of 2.052(1)–2.055(1) Å is similar to compound **3**. While viewed along the *c*-axis, the structure of compound **5a** appears to be rotated by ~90° to the next layer, resulting in the aforementioned kaleidoscope–type pattern.

Overall, the structure of **5a** forms a tight packing pattern with shorter distances between the metal(III) centers of neighboring molecules in comparison to its PFP counterpart compound **3**. The main in this compound is the participation of the substituted 4-position (butyloxy) with interactions to fluorine atoms rather than the pyrrole rings as seen in compound **3**. This results in more space around the fluorinated phenyl rings, causing the metal(III) centers to be closer

together, forming an attractive highly symmetric packing pattern.

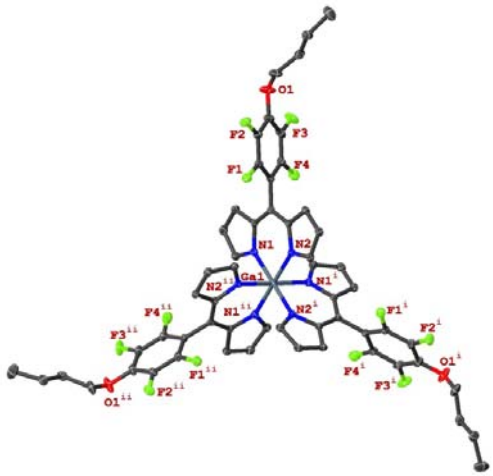

Figure 5. View of the molecular structure of complex **5a** in the crystal. Hydrogen atoms and labels for carbon atoms have been omitted. Thermal ellipsoids give 50% probability.

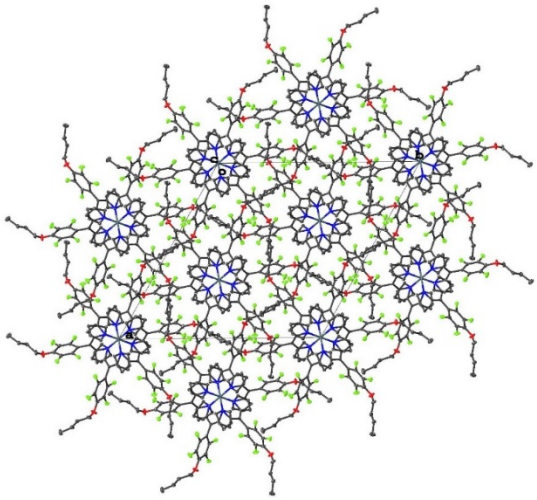

Figure 5a. View of the crystal packing of complex **5a** along the *c*-axis. Hydrogens atoms and atom labels have been omitted for clarity.

Similar test reactions of **2** and **3** with hexylamine under the conditions described for the reaction of amines with PFP substituents[10e] did not yield the desired amino-substituted complexes (see SI for details). There was either no reaction (**3**) or only partial reaction (**2**), i.e. a mixture of mono-, bis-, and tris-substituted complexes were obtained. A chromatographic separation of this mixture proved not to be possible.

However, the target complexes **10b**,**c**, **11a-c** were accessed by the reaction of the corresponding amino-functionalized dipyrrin ligands **6, 7** with the metal chlorides (Scheme 3). In a similar manner the alkoxy-substituted complexes **5a**,**b**, **12a**,**c**, and **13a**,**c** could also be obtained via the pre-functionalized dipyrrins **8** or **9**. These pre-functionalized dipyrrins were obtained by DDQ oxidation of the corresponding substituted dipyrranes.[12,13] Such pre-functionalized dipyrrins and dipyrranes have already been successfully employed for the synthesis of BODIPYs and other porphyrinoids.[12,13]

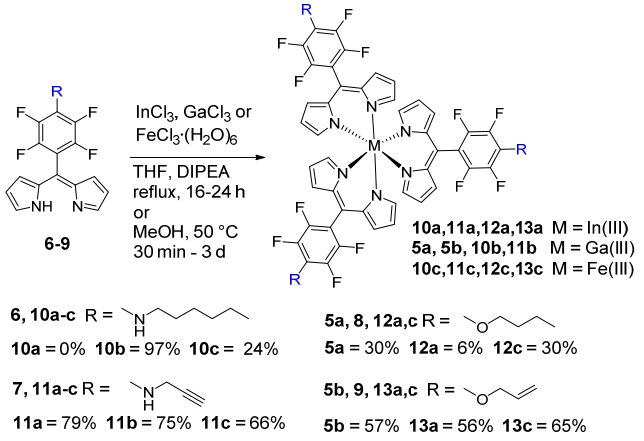

Scheme 3 Synthesis of tris(dipyrrinato) metal complexes via reaction of functionalized dipyrrins with the corresponding metal salts.

Two of the complexes, **12c** and **13a**, were characterized by single crystal X-ray crystallography (Figures 6 and 7). **12c** and **13a** were both solved with 1/3 of the molecule present in the asymmetric unit similar to that of **5a**. The structures of **12c** and **13a** show a similar F···H network as seen in compound **5a**. **12c** and **13a** have a similar artistic packing pattern as seen in compound **5a** while viewed along the *c*-axis with layers rotated by ~90° to each other, resulting in a kaleidoscope–type pattern, Figure 6a, and Figure 7a. The inclusion of an allyloxy (**13a**) group or a butyloxy (**12c**) group alters the F···H networks formed in comparison to the PFP compounds of **2** and **3**.

The structure of **12c** contains two major F···H contacts, C17–H17A···F2 (2.380(2) Å, 157.2(3)°), C2–H2···F4 (2.410(2) Å, 154.3(2)°). Just as in compound **5a** above the interactions are reciprocated and repeated three times over symmetry resulting in an extensive F···H network. The overall geometry of compound **12c** is an octahedral orientation of the ligands around the metal(III) center. There is a N–Fe–N angle range of 86.2(1)–91.8(1)° and a N–Fe bond length range of 1.964(3)–1.970(3) Å. Additionally, there is a Fe···Fe distance of 7.522(2) Å to the nearest neighboring molecule.

The structure of **13a** contains one major F···H contacts, C17–H17B···F4 (2.319(1) Å, 134.1(1)°), which, just like **5a** and **12c** above, is reciprocated and repeated three times due to symmetry. This results in the allyloxy chains being tethered to the fluorine groups of the phenyl ring through a F···H network. Additionally, the presence of a F···F short contact, F2···F4 (2.765(2) Å) results in an aggregation of phenyl rings within the unit cell. The overall geometry of compound **13a** is an octahedral orientation of the ligands around the metal(III) center. There is an N–In–N angle range of 83.6(1)–95.2(1)° and a N–In bond length range of 2.218(2)–2.221(2) Å. Additionally, there is an In···In distance of 7.564(2) Å to the nearest neighboring molecule.

Overall, the structures of **12c** and **13a** form a tight packing pattern. In comparison to PFP counterpart (**2**), compound **13a** displays a shorter distance between the metal(III) centers of neighboring molecules. The main difference between packing

of compound **13a** and **12c** with the PFP complexes **2** and **3**, is the participation of the substituted 4-position (**13a:** allyloxy, **12c:** butlyloxy) with interactions to fluorine groups rather than the pyrrole rings. As with compound **5a**, this results in more space around the fluorinated phenyl rings and causes the metal(III) centers to be closer together, forming an attractive high symmetric packing pattern.

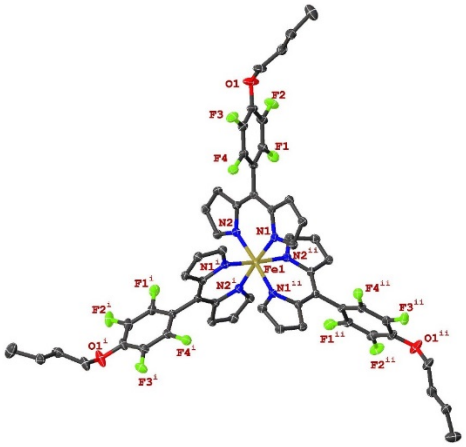

Figure 6. View of the molecular structure of complex **12c** in the crystal. Hydrogen atoms and labels for carbon atoms have been omitted. Thermal ellipsoids give 50% probability.

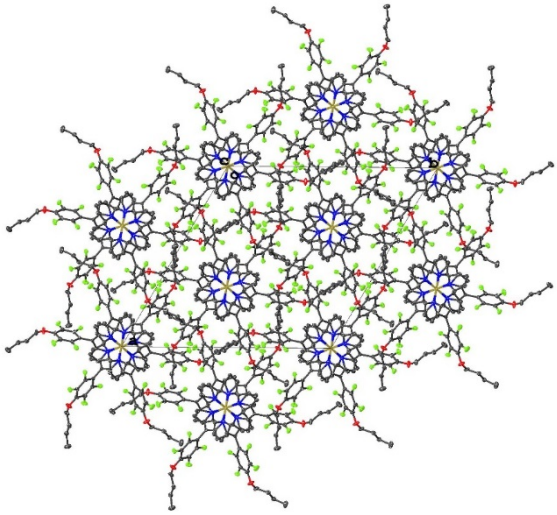

Figure 6a. View of the crystal packing of complex **12c** along the *c*-axis. Hydrogen atoms have been omitted for clarity.

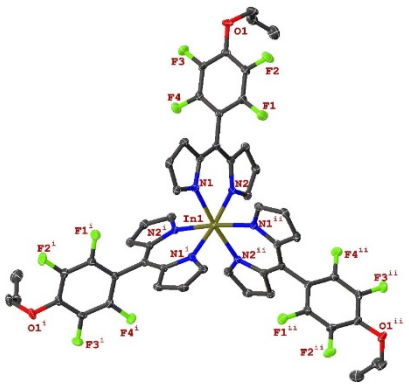

Figure 7. View of the molecular structure of complex **13a** in the crystal. Hydrogen atoms and labels for carbon atoms have been omitted. Thermal ellipsoids give 50% probability.

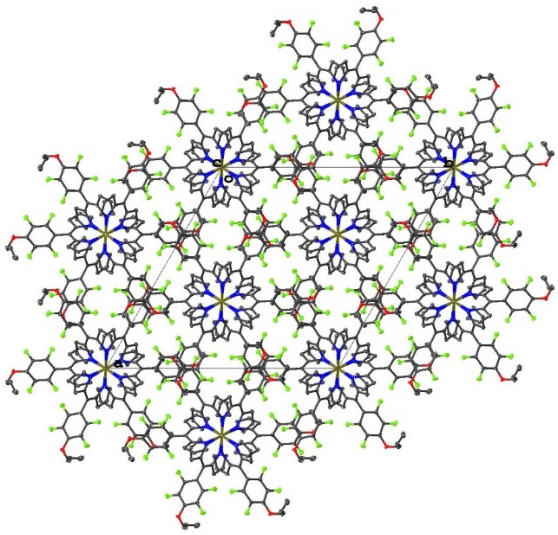

Figure 7a. View of the crystal packing of complex **13a** along the *c*-axis. Hydrogen atoms have been omitted for clarity.

Glycosylation is a valuable tool to increase the uptake of active moieties by cells and bacteria.[10,14] Glycosylation of porphyrinoids has extensively been applied to increase the bioavailability and efficacy of these compounds in the photodynamic therapy of tumors.[10a,e] In this respect, thiocarbohydrates have proven to be useful nucleophiles to achieve glycosylation of diverse substrates.[10a,e] Gallium(III) has garnered considerable interest as a chemotherapeutic agent *i.a.* based on its role as an antimetabolite to iron(III);[15] hence, complexes **3** and **4** were chosen for glycosylation experiments. The reaction of complexes **3** and **4** with the thiocarbohydrates 1-thio-β-D-glucose sodium salt or 1-thio-β-D-galactose sodium salt, respectively, yielded the desired glycosylated dipyrinato-complexes, **14a**,**b** and **15a**,**b** in all cases (Scheme 4). It is important to note that it would be difficult to obtain such glycosylated complexes via pre-functionalized ligands due to the sensitivity of the thiol linkage to oxidation. Under the strong oxidative conditions used for the preparation of the dipyrrin (DDQ), the thiol would be oxidized to the sulfone.[16] A possible nucleophilic substitution with thiocarbohydrates at the stage of the dipyrrin, on the other hand, would be impaired by the competing reactivity of *alpha*- and *para*-phenyl-position towards nucleophiles.[17] Moreover, the final assembly of the iron(III) complex would again require the strong oxidant $FeCl_3 \cdot 6H_2O$.

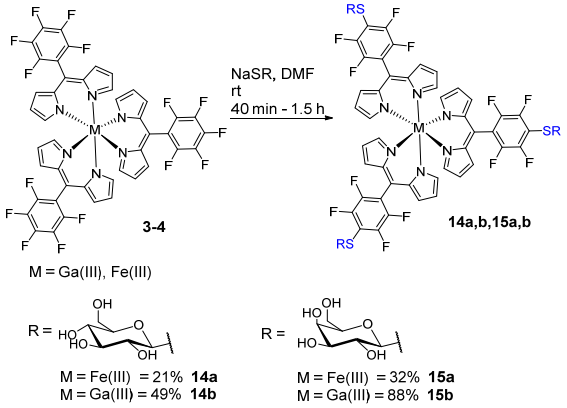

Scheme 4 Synthesis of glycosylated tris(dipyrrinato) complexes **14a**,**b** and **15a**,**b**.

Figure 8 shows the absorption spectra of the glucosylated gallium(III) complex **14b** in comparison with the butyloxy-substituted analogue **5a** and the parent complex **3**. Again there are only marginal differences between in the absorption spectra corresponding to the limited influence of the *para*-phenyl substituent on the basic chromophore.

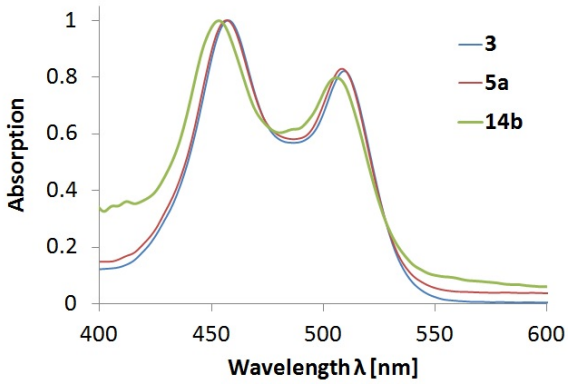

Figure 8. Absorption spectra (normalized) of complexes **3**, **5a** and **14b** in DCM (**3,5a**) and MeOH (**14b**).

As mentioned above there is increasing interest in ruthenium(II) and gallium(III) complexes as potential anti-tumor compounds.[4d,5c] Apart from their cytotoxic effects in the absence of light, their photoactivation has also come into focus.[18] Therefore it seemed reasonable to assess the photobiological properties of the new complexes. Hence, their (photo)cytotoxicity was tested on several tumor cell lines and against the bacterium *S. aureus*.

The toxicity of **14a**,**b** and **15a**,**b** in the absence and presence of light was evaluated in cellular assays in human epidermoid carcinoma A253, human epithelial carcinoma A431, human oral adenosquamous carcinoma CAL27, and colorectal adenocarcinoma HT29 cells (see Figures 9 and 10). In addition, the mouse fibroblast cell line L929 was tested as a non-tumorous cell line. The assays were carried out after incubation for 24 h, with the complexes in medium containing 10% fetal calf serum (FCS). Both, the cytotoxicity and the photocytotoxicity were determined at two different complex concentrations (2 and 10 µM). A white light source at a dose rate of approx. 50 J/cm^2 was used for irradiation. As seen in Figures 9 and 10 all compounds showed no or only very limited toxic effects in the absence of light. There is, however, a striking difference in the *photo*toxicity between the glycosylated gallium(III) and iron(III) complexes. Whereas the iron(III) complexes (**14a**, **15a**) show no or only very limited phototoxicity (**15a**, HT29 cell line), both gallium(III) complexes (**14b**, **15b**) exhibit a very high phototoxicity, even at lower concentration (2 µM). With the exception of the results with the HT29 cell line (**15b**), there seems to be no difference in the sensitivity of the four tumor cell lines to the phototoxic action of these gallium(III) complexes. This phototoxicity is also observed for the non-tumorous L929 fibroblast cell line, suggesting that the phototoxic activity is not related to some tumor-cell specific interaction. As a control experiment, the allyloxy-substituted gallium(III) complex **5b** (Figure 10, bottom) was also tested against the five cell lines and gave only very low phototoxicity (see Figure 10 below). This illustrates that the phototoxic activity is not simply due to the central metal ion but rather to the combination of metal ion and carbohydrate substitution. The literature on comparable metal complexes may suggest a phototoxicity *via* type I or type II photoreactions.[18a-c] However, the exact mechanism of this phototoxicity remains to be elucidated. For ruthenium(II) complexes other mechanisms like a photodissociation of ligands have been proposed.[18d-f]

Journal Name

ARTICLE

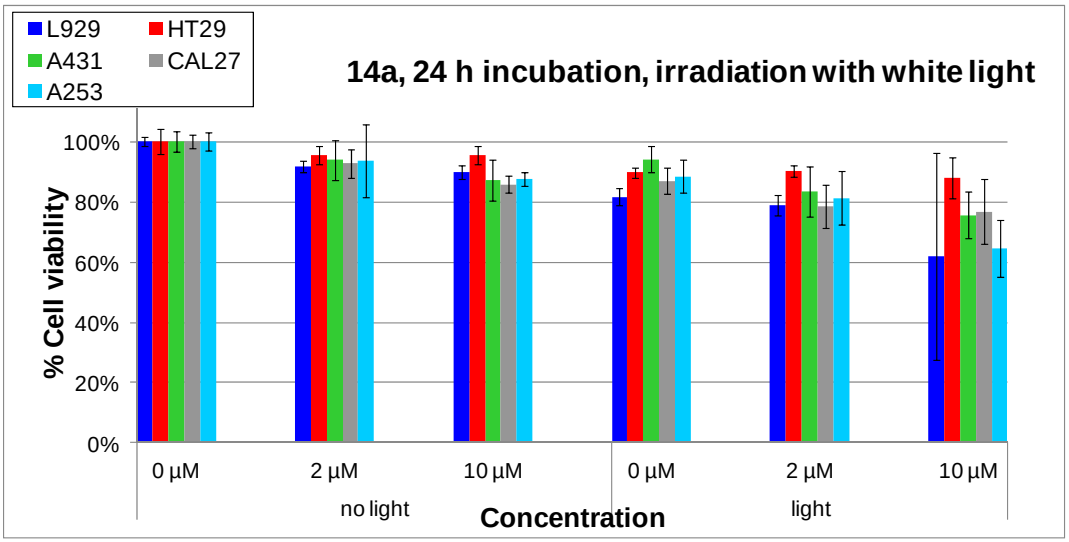

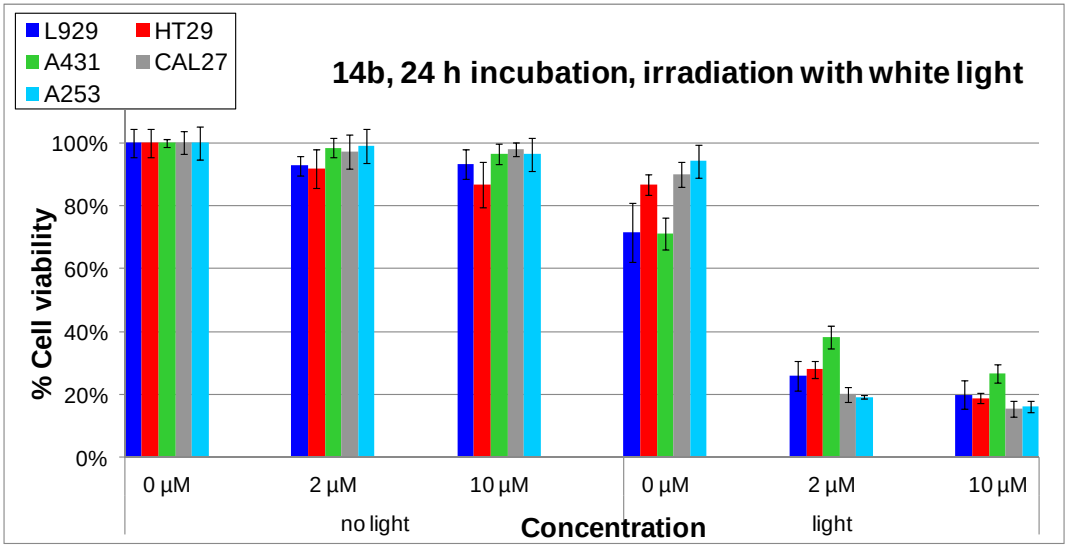

Figure 9. Phototoxicity of **14a**,**b** (glucose-substituted complexes) in cellular assays with the L929, A431, A253, HT29 and CAL27 cell lines.

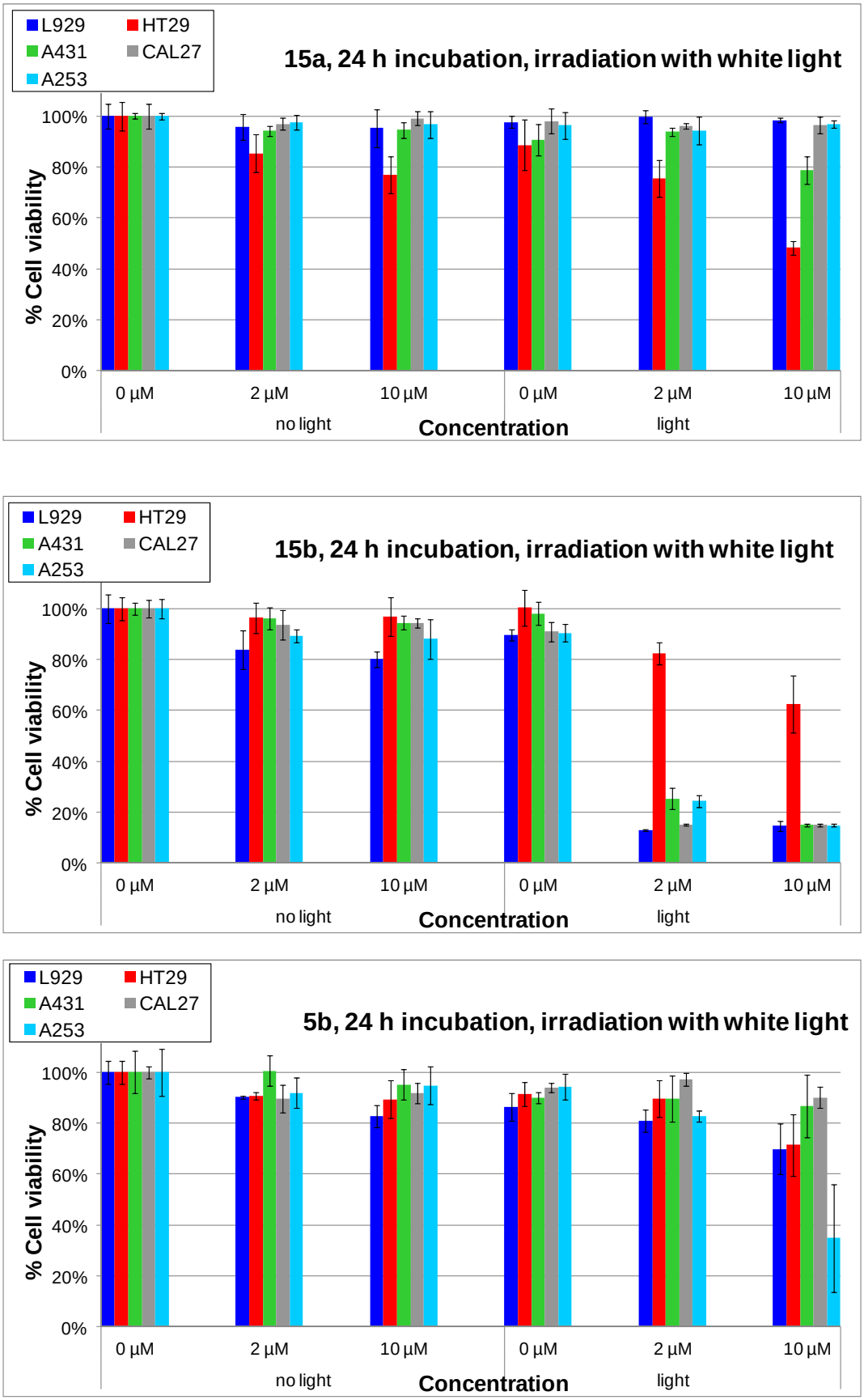

Figure 10. Phototoxicity of **15a,b** (galactose-substituted complexes) and **5b** (allyloxy-substituted gallium(III) complex) in cellular assays with the L929, A431, A253, HT29 and CAL27 cell lines.

Another field of application for photoactive substances is the photodynamic inactivation of bacteria.[19] Thus, complexes **5b**, **14a**,**b** and **15a**,**b** were tested against *S. aureus,* a common standard in the investigation of antibacterial activity and a typical Gram-positive member of the microflora of infected wounds.[20] Cultures of *S. aureus* were incubated with the complexes for 30 min in three different concentrations (1, 10, and 100 µM). A white light source at a dose rate of approx. 100 J/cm^2 was used for irradiation (see SI for details). The activity pattern of the complexes against *S. aureus* was very similar to that found in the tumor cells (Figures 11 and 12); High phototoxicity of the glycosylated gallium(III) complexes (**14b**, **15b**) but no activity of the glycosylated iron(III) complexes (**14a**, **15a**) and the allyloxy-substituted gallium(III) complex (**5b**). For both gallium(III) complexes – even at the lowest concentration of 1 µM – after white light irradiation, a complete inactivation of *S. aureus* was observed corresponding to a six log reduction of the bacteria.

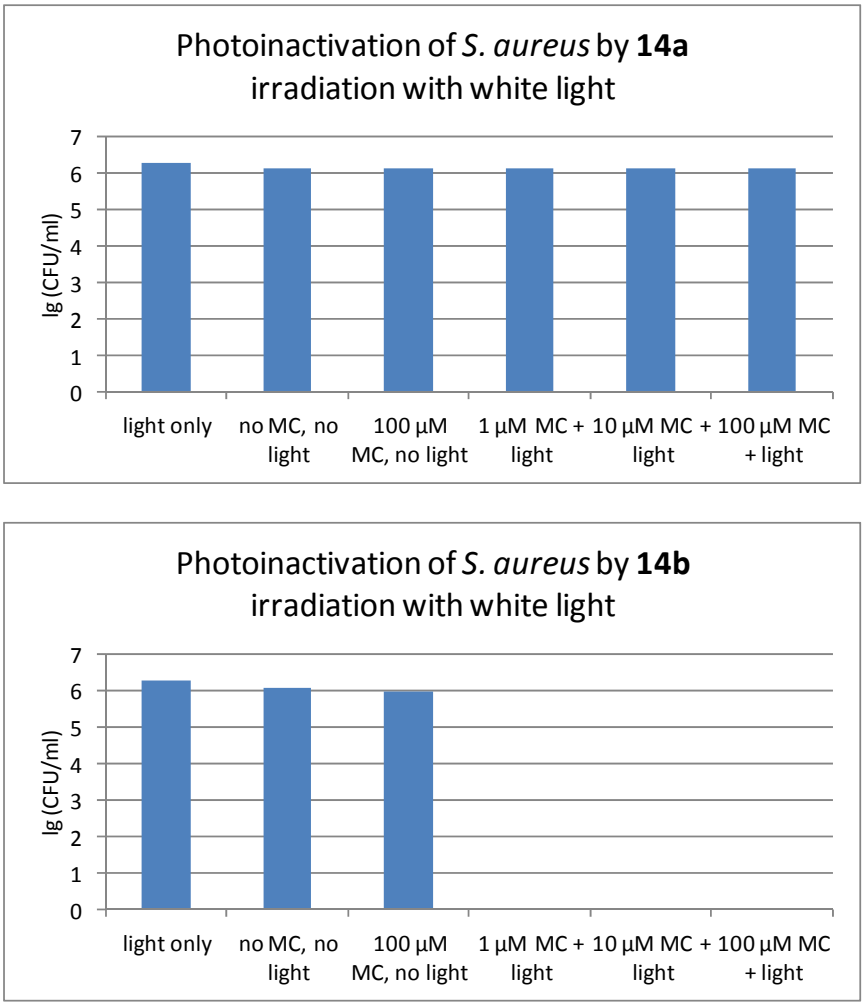

Figure 11. Photoinactivation of *S. aureus* by **14a**,**b** (glucose-substituted complexes) in phosphate-buffered saline (PBS) (30 min incubation, irradiation with white light), MC = metal complex, given is the logarithm of the number of colony-forming units, lg (CFU/ml). For **14b** under light irradiation for all three concentrations, a complete inactivation of the bacteria is observed.

Journal Name

ARTICLE

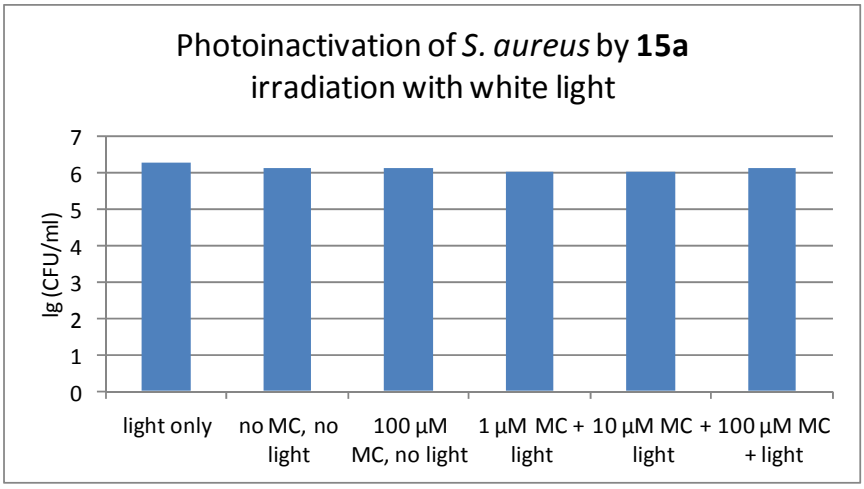

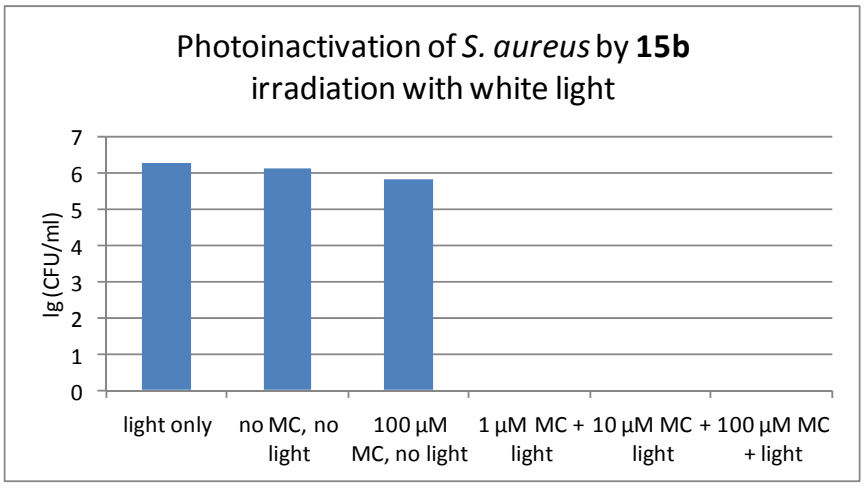

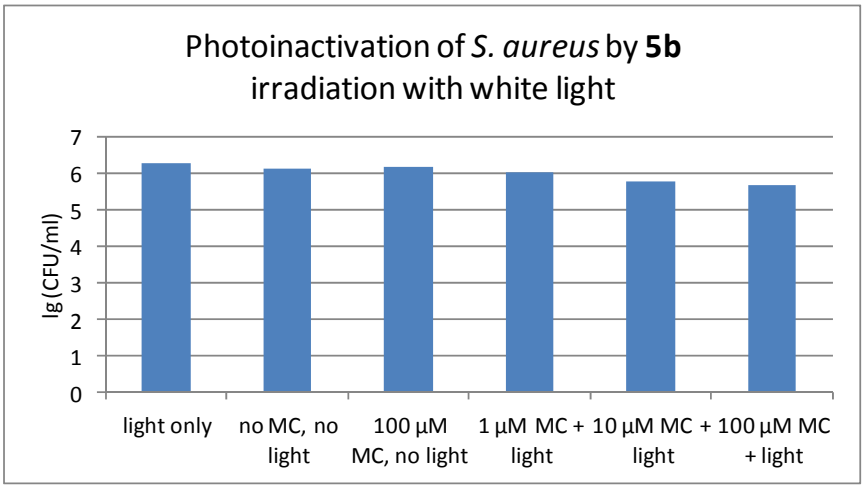

Journal Name

ARTICLE

Figure 12. Photoinactivation of *S. aureus* by **15a**,**b** (galactose-substituted complexes) and **5b** (allyloxy-substituted gallium(III) complex) in phosphate-buffered saline (PBS) (30 min incubation, irradiation with white light), MC = metal complex, given is the logarithm of the number of colony-forming units, lg (CFU/ml). For **15b** under light irradiation for all three concentrations, a complete inactivation of the bacteria is observed.

The last step was to expand the synthetic concept also to other metal complexes. Due to their medical relevance[4d,18c] ruthenium(II) complexes were chosen. As starting point the well-known dichloro(*p*-cymen)ruthenium(II) dimer[21] **16** was reacted with PFP-dipyrrin **1** to obtain the [(η^6-p-cymen)ruthenium(Cl)(5-pentafluorophenyl)dipyrrin)] [**17**].[22] Reaction with 2,2'-bipyridine afforded the new PFP-substituted ruthenium(II) complex **18** (Scheme 5).[8d,22,23]

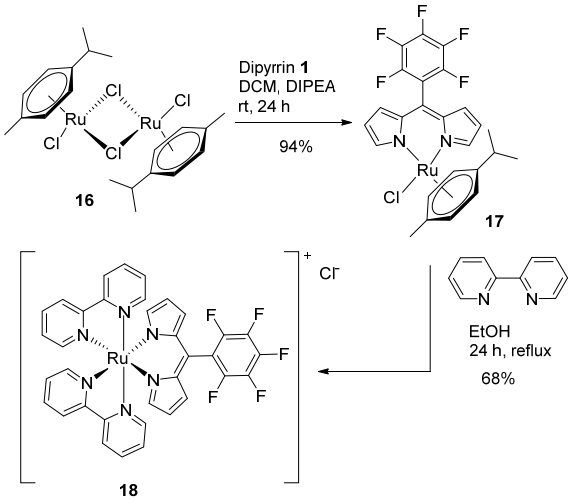

Scheme 5. Synthesis of PFP-substituted ruthenium(II) complex **18**.

Using the conditions employed above, **18** was functionalized *via* S_NAr with allyl and propargyl alcohol, as well as allyl amine and propargyl amine to obtain the alkoxy-substituted ruthenium(II) complexes **19a**,**b** and the amino-substituted complexes **20a**,**b** in acceptable yields (Scheme 6).

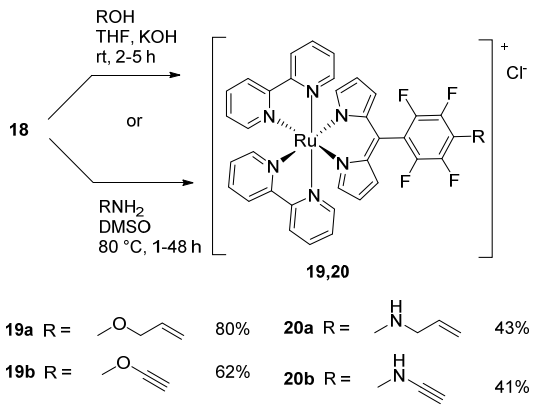

Scheme 6. Substitution of complex **18** with nucleophiles.

Finally, the thioglycosylation proved to be transferable to ruthenium(II) complexes, the thioglycosylated complex **21** being isolated in 50% yield after just 10 min reaction time (Scheme 7).

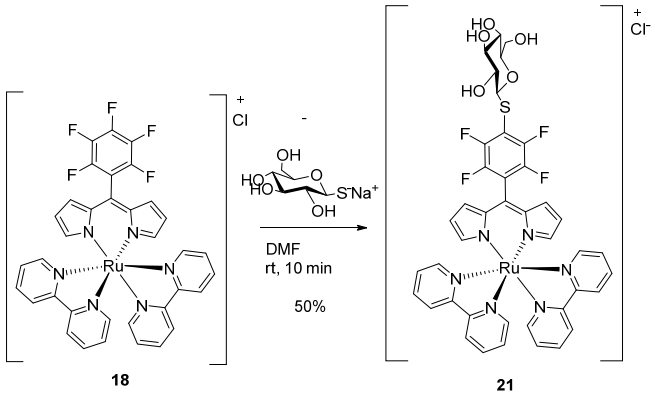

Scheme 7 Post-functionalization of a dipyrrinato ruthenium(II) complex with thioglucose.

These examples illustrate the versatility of the current approach to obtain functionalized metal complexes using the PFP moiety as an anchor for S_NAr reactions with nucleophiles.

Conclusions

In conclusion, the post-functionalization of tris(dipyrrinato) complexes of gallium(III), indium(III), and iron(III) carrying pentafluorophenyl moieties with alcohols and thiocarbohydrates has been achieved. Using this synthetic route, metal complexes with sensitive functional groups are available in a facile manner and good yields. For the less sensitive alkoxy-groups, the complexes can also be prepared with the corresponding pre-functionalized dipyrrins. It is shown that this synthetic approach is also applicable to other metal complexes giving access to functionalized ruthenium(II) complexes. Selected complexes were tested for their (photo)cytotoxicity in cellular assays against tumor cell lines and against the bacterium *S. aureus*. Phototoxic activity against tumor cells as well as against *S. aureus* was predominantly observed with the glycosylated gallium(III) complexes. The phototoxic activity appears to be dependent on the metal as well as on the carbohydrate unit present. The specific mechanism of phototoxic action, as well as the post-

functionalization with other (thio)carbohydrates and biomolecules, will be elucidated in future studies.

This project has received funding from the European Union's Horizon 2020 research and innovation programme under the Marie Skłodowska-Curie Grant Agreement No. 764837 and was supported by a grant from Science Foundation Ireland (IvP 13/IA/1894) (M.O.S.). The biolitec research GmbH gratefully acknowledges financial support by the German Bundesministerium für Bildung und Forschung (BMBF) (project "Response-FV9", FKZ 03ZZ0914I).

Experimental Section

General

The nomenclature and numbering (^{13}C and ^{19}F NMR spectra) are in accordance with IUPAC recommendations. THF and DMF used as solvents for the reactions were stored over molecular sieves. All liquid reagents were added through syringes. Purchased reagents were used as received without further purification. All reactions were monitored by TLC analysis. The preparative purification of mixtures by column chromatography was conducted on silica gel (60 M, 40-63 µm). The yields refer to analytically pure compounds. NMR spectra were recorded on a 400 and 500 MHz instrument, respectively. Chemical shifts are given in parts per million (ppm**)** relative to the resonance of the solvent. As deuterated solvents chloroform (δ = 7.26, 77.0 ppm) and methanol (δ = 3.31, 49.0 ppm) were used. Integrals are in accordance to assignments and coupling constants are given in hertz (Hz). All ^{13}C NMR spectra are proton–decoupled. The multiplicity is indicated as follows: s (singlet), br s (broad singlet), d (doublet), t (triplet), m (multiplet), m_c (centered multiplet) dd (doublet of doublets). The *ortho*- and *meta*-fluorine signals in the ^{19}F NMR spectra of the substituted tetrafluorophenyl moieties exhibit the A,A'B,B' and A,A'X,X' coupling pattern typical for *para*-substituted aromatic compounds, in the ^{19}F NMR spectra these signals are denoted as m_c. HRMS analyses were performed by ESI-TOF, the solvent flow rate was adjusted to 4 µL/min and spray voltage was set to 4 kV. Drying gas flow rate was set to 15 psi (1 bar) and all other parameters were adjusted for a maximum abundance of the respective $[M+H]^+$. The UV/Vis spectra were measured with a UV/Visible spectrometer using DCM as solvent and quartz cuvettes of 1 cm length. Emission spectra were recorded with a fluorescence spectrometer using quartz cuvettes of 1 cm length and DCM as a solvent. Melting points are uncorrected. Compounds **1**[7c], 5-{4-(*N*-hexylamino)-2,3-5,6-tetrafluorophenyl}-dipyrrane[12], 5-{4-(*N*-prop-2-ynylamino)-2,3,5,6-tetrafluorophenyl}-dipyrrane[12], 5-{4-(prop-2-ynyloxy)-2,3,5,6-Tetrafluorophenyl}-dipyrrane[13], 5-{4-(butyl-1-oxy)-2,3,5,6-tetrafluorophenyl}-dipyrrane[13], and dichloro(*p*-cymen)ruthenium(II) dimer[21] [**16**] were prepared according to the literature**.**

Synthetic procedures

Synthesis of tris(5-pentafluorophenyl-dipyrrinato) indium(III) [2] and tris(5-pentafluorophenyl-dipyrrinato) gallium(III) [3]: Under argon atmosphere PFP-dipyrrin **1** (3.1 eq) was dissolved in dry THF, $InCl_3$ or $GaCl_3$ and DIPEA (14 eq) were added and the reaction mixture was refluxed for 6 h. After cooling to rt the solvent was evaporated, purified by column chromatography (silica gel, DCM) and recrystallization (DCM/*n*-hexane) to obtain the product as orange crystals. The products were analyzed by ^{1}H, ^{13}C, ^{19}F NMR spectroscopy, HRMS, melting point, elemental analysis, and UV/Vis spectroscopy.

Synthesis of tris(5-pentafluorophenyl-dipyrrinato)iron(III) [4]: Under argon atmosphere PFP-dipyrrin **1** (100 mg, 0.32 mmol, 3.1 eq) was dissolved in dry MeOH (10 mL), $FeCl_3 \cdot 6\ H_2O$ (27 mg, 0.10 mmol) and DIPEA (0.24 mL, 186 mg, 1.44 mmol, 14 eq) were added and the mixture was stirred for 30 min at 50 °C. The mixture was diluted with DCM and washed several times with water. The organic layer was dried with sodium sulfate, filtered and evaporated to dryness. The crude product was purified by column chromatography (silica gel, DCM) and washed with pentane to obtain the product as a black solid (60 mg, 61%). The data are in accordance with the literature.[7b]

General procedure for the post-functionalization of 3 with alcohols (complexes 5a-c): Under argon atmosphere complex **3**, freshly powdered KOH (30 eq) and the specific alcohol (20 eq) in dry THF were stirred at rt for 16 h. The mixture was diluted with DCM, washed several times with water and the organic layer was dried with sodium sulfate, filtered and evaporated to dryness. The crude product was purified by column chromatography (silica gel, DCM/*n*-hexane = 1:1) and washed with pentane to obtain the product as an orange solid. The products were analyzed by ^{1}H, ^{13}C, ^{19}F NMR spectroscopy, HRMS, melting point, and UV/Vis spectroscopy.

General procedure for the synthesis of *para*-phenyl-substituted PFP-dipyrrins 6-9: A mixture of *para*-phenyl-substituted PFP-dipyrrane[12,13] and DDQ (1.3 eq) in THF was stirred for 20 min at rt. The mixture was filtered through silica gel and evaporated to dryness. Further purification was achieved by column chromatography (silica gel, DCM) to obtain the product as a yellow oil. The products were analyzed by ^{1}H, ^{13}C, ^{19}F NMR spectroscopy, HRMS, and UV/Vis spectroscopy.

General procedure for the synthesis of tris(dipyrrinato) complexes starting from pre-functionalized dipyrrins:

a) Synthesis of indium(III) and gallium(III) complexes 10a, 11a, 12a, 13a, 5a,b 10b and 11b: Under argon atmosphere a mixture of dipyrrin (3.1 eq), $InCl_3$ (1 eq) or $GaCl_3$ (1 eq) and DIPEA (3.1 eq) were dissolved in THF and refluxed for the specific time (see SI). After cooling to rt the mixture was diluted with DCM and washed several times with water. The organic layer was dried with sodium sulfate, filtered and evaporated to dryness. The crude product was purified by column chromatography (see SI for the specific solvent mixture), washed with pentane to obtain the product as orange crystals. The products were analyzed by ^{1}H, ^{13}C, ^{19}F NMR spectroscopy, melting point, HRMS, and UV/Vis spectroscopy.

b) Synthesis of iron(III) complexes 10a-c: Under argon atmosphere dipyrrin (3.1 eq) was dissolved in dry MeOH; $FeCl_3 \cdot 6\ H_2O$ (1 eq) and DIPEA (14 eq) were added and the mixture was stirred for 30 min at 50 °C. After cooling to rt the mixture was evaporated to dryness, purified by column chromatography (see SI for the specific solvent mixture) and washed with pentane to obtain the product as a green solid. The products were analyzed by ^{1}H, ^{19}F NMR spectroscopy, melting point, HRMS, and UV/Vis spectroscopy.

General procedure for the synthesis of the glycosylated metal complexes 14a,b and 15a,b: Under argon atmosphere and exclusion of light complex **3** or **4** was dissolved in dry DMF, the specific thiocarbohydrate sodium salt (4.5 eq) was added and the mixture stirred for a specific time (details see in SI) at rt. The mixture was evaporated to dryness, purified by column chromatography (silica gel, DCM/MeOH = 85:15) and washed with pentane to obtain the product as a solid. The products were analyzed by ^{1}H, ^{13}C, ^{19}F NMR spectroscopy, melting point, HRMS, and UV/Vis spectroscopy.

General procedure for the post-functionalization of complex 18 with alcohols: Under argon atmosphere and exclusion of light complex **18** was dissolved in dry THF, freshly powdered KOH (1.3 eq) and the specific alcohol (2 eq) was added and the mixture was stirred for a specific time (details see in SI) at rt. The mixture was diluted with DCM and washed with water several times. The organic layer was dried with sodium sulfate, filtered and evaporated to dryness. The crude product was purified by column chromatography (silica gel, DCM/MeOH = 85:15) and recrystallization (DCM/*n*-pentane) to obtain the product as solid. The products were analyzed by ^{1}H, ^{13}C, ^{19}F NMR spectroscopy, melting point, HRMS, and UV/Vis spectroscopy.

General procedure for the post-functionalization of complex 18 with amines: Under argon atmosphere complex **18** was dissolved in dry DMSO, amine (20 eq.) was added and the mixture was stirred for a specific time (details see in SI) at 80 °C. The mixture was diluted with DCM, washed with water, dried with sodium sulfate, filtered and evaporated to dryness. The crude product was purified by column chromatography (silica gel, DCM/MeOH = 85:15) to obtain the product as solid. The products were analyzed by ^{1}H, ^{13}C, ^{19}F NMR spectroscopy, melting point, HRMS, and UV/Vis spectroscopy.

Synthesis of glycosylated ruthenium(II) complex 21: Under argon atmosphere and the exclusion of light complex **18** (100 mg, 0.13 mmol) was dissolved in dry DMF (3 mL), 1-thio-β-D-glucose sodium salt hydrate (37 mg, 0.17 mmol, 1.3 eq) was added and the mixture stirred for 10 min at rt. The mixture was evaporated to dryness and purified by column chromatography (DCM/MeOH = 85:15) to obtain the product as black solid (60 mg, 50%). The product was analyzed by ^{1}H, ^{13}C, ^{19}F NMR spectroscopy, melting point, HRMS, and UV/Vis spectroscopy.

Materials and Methods

Cell testing

Human epidermoid carcinoma A253, human epithelial carcinoma A431, human oral adenosquamous carcinoma CAL27, L929 mouse fibroblast, and colorectal adenocarcinoma HT29 cells were grown in Dulbecco's modified eagle medium (DMEM) with 10% heat inactivated FCS, 1% penicillin (10000 IU) and streptomycin (10000 µg mL^{-1}). A stock solution (2 mM) of the metal complex was prepared at 4 °C in DMSO and kept in the dark. DMEM (without phenol red) with 10% FCS was used for further dilution to reach a concentration of 2 or 10 µM of the metal complex, respectively. In microplates 2 × 104 cells per well were seeded in fresh medium (DMEM without phenol red) containing 10% FCS with 2 µM or 10 µM of the metal complex and incubated for 24 h. After an exchange of medium (to remove any metal complex not taken up by the cells), the irradiation was performed at RT with a white light source [KL 2500 LCD (Schott)] at a dose rate of app. 50 J cm^{-2}. The cell viability of the samples was assessed using the XTT assay[6] and the absorbance was measured with a Tecan Infinite 200 microplate reader, at a wavelength of 490 nm.

Bacterial testing

The bacterium *S. aureus* DSM11729 is a typical Gram-positive member of the wound microflora. Cultured bacterial cells were suspended in sterile PBS, or sterile PBS supplemented with 10% sterile horse blood serum. The final OD (optical density) at 600 nm (1 cm cuvette path length) in all cases was 0.015. The bacterial suspensions were placed in sterile black well plates with clear bottoms. Concentrations of metal complexes used in the study were 100 µM, 10 µM, and 1 µM. After an incubation time of 30 min at rt, the samples were irradiated with a white light source [KL 2500 LCD (Schott)] at a dose rate of approximately 100 J cm^{-2}. Control plates containing no metal complex were not exposed to light. The control samples for dark toxicity were only exposed to metal complex without any illumination.

Crystallography

Crystals were grown following the protocol developed by Hope by dissolving the compounds in either DCM or a DCM/MeOH mixture and allowing for slow evaporate over time and handled as described before.[23] Single crystal X-ray diffraction data for all compounds were collected on a Bruker APEX 2 DUO CCD diffractometer by using graphite-monochromated MoK_α (λ = 0.71073 Å) radiation and Incoatec IμS CuK_α (λ = 1.54178 Å) radiation. Crystals were mounted on a MiTeGen MicroMount and collected at 100(2) K by using an Oxford Cryosystems Cobra low-temperature device. Data were collected by using omega and phi scans and were corrected for Lorentz and polarization effects by using the APEX software suite.[24] Using Olex2, the structure was solved with the XT structure solution program, using the intrinsic phasing solution method and refined against |F2| with XL using least squares minimization.[25] Hydrogen atoms were generally placed in geometrically calculated positions and refined using a riding model. Details of data refinements can be found in Table S1 and S2 and further experimental and refinement detail can be found in the SI. All images were prepared by using Olex2.[25a]

CCDC-1841033 (for **2**), -1841036 (for **3**), -1841035 (for **5a**), -1841033 (for **12c**), and -1841032 (for **13a**) contains the supplementary crystallographic data for this paper. These data sets

can be obtained free of charge from The Cambridge Crystallographic Data Center via http://www.ccdc.cam.ac.uk/data_request/cif.

Conflicts of interest

There are no conflicts to declare.

Notes and references

1 (*a*) K. Dralle Mjos and C. Orvig, *Chem. Rev.,* 2014, **114**, 4540−4563; (*b*) C. G. Hartinger and P. J. Dyson, *Chem. Soc. Rev.,* 2009, **38**, 391–401; (*c*) T. Storr, K. H. Thompson and C. Orvig, *Chem. Soc. Rev.,* 2006, **35**, 534–544; (*d*) K. H. Thompson and C. Orvig, *Science,* 2003, 936–939; (*e*) Z. Guo and P. Sadler *J. Angew. Chem. Int. Ed.,* 1999; **38**, 1512–1531; *Angew. Chem.,* 1999, **111**, 1610–1630; (*f*) M. J. Clarke, F. Zhu and D. R. Frasca, *Chem. Rev.*, 1999, **99**, 2511–2533.

2 (*a*) M. Zaki, F. Arjmand and S. Tabassum, *Inorg. Chim. Acta*, 2016, **444**, 1–22; (*b*) L. Ronconi and P. J. Sadler, *Coord. Chem. Rev.,* 2007, **251**, 1633–1648; (*c*) T. W. Hambley, *Dalton Trans.,* 2007, 4929–4937.

3 (*a*) A. Bergamo, P. J. Dyson and G. Sava, *Coord. Chem. Rev.*, 2018, **360**, 17–33; (*b*) E. Wexselblatt, E. Yavin and D. Gibson, *Inorg. Chim. Acta,* 2012, **393**, 75–83; (*c*) N. J. Wheate, S. Walker, G. E. Craig and R. Oun, *Dalton Trans.*, 2010, **39**, 8113–8127; (*d*) Y. Jung and S. J. Lippard, *Chem. Rev.,* 2007, **107**, 1387–1407; (*e*) D. Wang and S. J. Lippard, *Nat. Rev. Drug Disc.,* 2005, **4**, 307–320; (*f*) M. A. Fuertes, C. Alonso and J. M. Pérez, *Chem. Rev.,* 2003, **103**, 645–662; (*g*) E. Wong and C. M. Giandomenico, *Chem. Rev.,* 1999, ***99,*** 2451–2466; (*h*) E. R. Jamieson and S. J. Lippard, *Chem. Rev.,* 1999, **99***,* 2467–2498; (*i*) J. Reedijk, *Chem Commun.,* 1996, 801–806.

4 (*a*) M. A. Jakupec, M. Galanski, V. B. Arion, C. G. Hartinger and B. K. Keppler, *Dalton Trans.*, 2008, 183–194; (*b*) M. J. Clarke, *Coord. Chem. Rev.,* 2003, **236**, 209–233; (*c*) S. Allardyce and P. J. Dyson, *Platinum Met. Rev.,* 2001, **45**, 62–69; (*d*) M. Hanif and C. G. Hartinger, Ruthenium Anticancer Agents En Route to the Tumor: From Plasma Protein Binding Agents to Targeted Delivery, In: A. A. Holder, L. Lilge, W. R. Browne, M. A. W. Lawrence and J. L. Bullock Jr. (Eds.), Ruthenium Complexes – Photochemical and Biomedical Applications (pp. 161–180), Wiley, Weinheim, 2018.

5 (*a*) T. Gianferrara, I. Bratsos and E. Alessio, *Dalton Trans.,* 2009, 7588–7598; (*b*) L. R. Bernstein, *Pharmacol. Rev.,* 1998, **50**, 665–682; (*c*) C. R. Chitambar, Gallium Complexes as Anticancer Drugs, In: A. Sigel, H. Sigel, E. Freisinger and R. K. O. Sigel (Eds.), Metallo-Drugs: Development and Action of Anticancer Agents (pp. 281–302), De Gruyter, Berlin/Boston 2018; (*d*) J. A. Lessa, G. L. Parrilha and H. Beraldo, *Inorg. Chim. Acta*, 2012, **393**, 53–63.

6 T. E. Wood and A. Thompson, *Chem. Rev.* 2007, **107**, 1831–1861. The origin of dipyrrin chemistry dates back to Hans Fischer's work in the beginning of the 20th century, see e.g. H. Fischer and H. Orth, Die Chemie des Pyrrols, Akademische Verlagsgesellschaft, Leipzig, 1937.

7 (*a*) S. Das and I. Gupta, *Inorg. Chem. Commun.,* 2015, **60**, 54–60; (*b*) J.-Y. Shin, B. O. Patrick, S. B. Son, J. R. Hahn and D. Dolphin, *Bull. Korean Chem. Soc.,* 2010, **31**, 1004–1013; (*c*) L. Yu, K. Muthukumaran, I. V. Sazanovich, C. Kirmaier, E. Hindin, J. R. Diers, P. D. Boyle, D. F. Bocian, D. Holten and J. S. Lindsey, *Inorg. Chem.,* 2003, **42**, 6629–6647; (*d*) C. Brückner, V. Karunaratne, S. J. Rettig and D. Dolphin, *Can. J. Chem.,* 1996, **74**, 2182–2193; (*e*) H. Fischer and M. Schubert, *Ber. Dtsch. Chem. Ges.,* 1924, **57**, 610–617.

8 (*a*) S. A. Baudron, *Dalton Trans.,* 2013, **42**, 7498–7509; for recent examples see: (*b*) S. Kusaka, R. Sakamoto and H. Nishihara, *Inorg. Chem.,* 2014, **53**, 3275–3277; (*c*) G. Li, L. Ray, E. N. Glass, K. Kovnir, A. Khoroshutin, S. I. Gorelsky and M. Shatruk, *Inorg. Chem.,* 2012, **51**, 1614–1624; (*d*) S. J. Smalley, M. R. Waterland and S G. Telfer, *Inorg. Chem.,* 2009, **48,** 13–15; (*e*) J. R. Stork, V. S. Thoi and S. M. Cohen, *Inorg. Chem.,* 2007, **46**, 11213–11223; (*f*) V. S. Thoi, J. R. Stork, D. Magde and S. M. Cohen, *Inorg. Chem.,* 2006, **45**, 10688–10697; (*g*) D. L. Murphy, M. R. Malachowski, C. F. Campana and S. M. Cohen*, Chem. Commun.,* 2005, 5506–5508; (*h*) S. R. Halper and S. M. Cohen, *Inorg. Chem.,* 2005, **44**, 486–488; (*i*) C. Brückner, Y. Zhang, S. J. Rettig and D. Dolphin, *Inorg. Chim. Acta*, 1997, **263**, 279–286.

9 (*a*) S. J. Garibay, J. R. Stork, Z. Wang, S. M. Cohen and S. G. Telfer, *Chem. Commun*., 2007, 4881–4883; (*b*) S. R. Halper, L. Do, J. R. Stork and S. M. Cohen, *J. Am. Chem. Soc.,* 2006, **128**, 15255–15268.

10 (*a*) S. Singh, A. Aggarwal, N. V. S. Dinesh, K. Bhupathiraju, G. Arianna, K. Tiwari and C. M. Drain, *Chem. Rev.*, 2015, **115**, 10261−10306; (*b*) C. Moylan, E. M. Scanlan and M. O. Senge, *Curr. Med. Chem.*, 2015, **22**, 2238−2348; (*c*) T. W. Johnson, K. R. Dress and M. Edwards, *Bioorg. Med. Chem. Lett.,* 2009, **19**, 5560–5564; (*d*) C. G. Hartinger, A. A. Nazarov, S. M. Ashraf, P. J. Dyson and B. K. Keppler, *Curr. Med. Chem.*, 2008, **15**, 2574–2591; for recent examples see (*e*) N. V. S. Dinesh K. Bhupathiraju, W. Rizvi, J. D. Batteas and C. M. Drain, *Org. Biomol. Chem*., 2016, **14**, 389–408; (*f*) J. Möker and J. Thiem, *Carbohydr. Res.,* 2012, **348**, 14–26; (*g*) J. Möker, U. Salge-Bartels and J. Thiem, *J. Carbohydr. Chem*., 2012*,* **31***, 702–710*; (*h*) J. Möcker and J. Thiem, *Eur. J. Org. Chem.,* 2009, 4842–4847; (*i*) D. L. Ma, T. Y. T. Shum, F. Y. Zhang, C. M. Che and M. S. Yang, *Chem. Commun.,* 2005, 4675–4677; (*j*) Y. S. Chen, M. J. Heeg, P. G. Braunschweiger, W. H. Xie and P. G. Wang, *Angew. Chem. Int. Ed.*, 1999, **38**, 1768–1769; *Angew. Chem.*, 1999, **111**, 1882–1884.

11 (*a*) S. Guski, M. Albrecht, T. Willms, M. Albrecht, T. Nabeshima, F. Pan, R. Puttreddy and K. Rissanen, *Chem Commun.,* 2017, **53**, 3213–3215 (To the best of our knowledge this is the first example of a glycosylated dipyrrin); (*b*) D. Perl, S. W. Bisset and S. G. Telfer, *Dalton Trans.,* 2016, **45**, 2440–2443.

12 C. S. Gutsche, M. Ortwerth, S. Gräfe, K. J. Flanagan, M. O. Senge, H.-U. Reissig, N. Kulak and A. Wiehe, *Chem. Eur. J.,* 2016, **22**, 13953–13964.

13 H. R. A. Golf, H.-U. Reissig and A. Wiehe, *Org. Lett.*, 2015, **17**, 982−985.

14 (*a*) M. G. Vander Heiden, L. C. Cantley and C. B. Thompson, *Science,* 2009, **324**, 1029−1033; (*b*) R. E. Airley and A. Mobasheri, *Chemotherapy*, 2007, **53**, 233−256; (*c*) O. Warburg, *Science*, 1956, **123**, 309–314.

15 (*a*) F. Minandri, C. Bonchi, E. Frangipani, F. Imperi and P. Visca, *Future Microbiol.,* 2014, **9**, 379–397; (*b*) C. R. Chitambar, *Biochim. Biophys. Acta*, 2016, **1863**, 2044–2053.

16 (*a*) P. Pasetto, X. Chen, C. M. Drain and R. W. Franck, *Chem. Commun.*, 2001, 81–82; (*b*) L. B. Poole, *Free Radical Biol. Med.*, 2015, **80**, 148–157; (*c*) G. A. Bagiyan, I. K. Koroleva, N. V. Soroka, and A. V. Ufimtsev, *Russ. Chem. Bull., Int. Ed.*, 2003, **52**, 1135–1141; (*d*) M. Musiejuk, T. Klucznik, J. Rachon and D. Witt, *RSC Adv.*, 2015, **5**, 31347–31351.

17 C. S. Gutsche, B. F. Hohlfeld, K. J. Flanagan, M. O. Senge, N. Kulak, and A. Wiehe, *Eur. J. Org. Chem.*, 2017, 3187–3196.

18 (*a*) F. Heinemann, J. Karges and G. Gasser, *Acc. Chem. Res.*, 2017, **50**, 2727–2736; (*b*) C. Mari, V. Pierroz, S. Ferrari and G. Gasser, *Chem. Sci.*, 2015, **6**, 2660–2686; (*c*) L. Lilge, Use of Ruthenium Complexes as Photosensitizers in Photodynamic Therapy, In: A. A. Holder, L. Lilge, W. R. Browne, M. A. W. Lawrence and J. L. Bullock Jr. (Eds.), Ruthenium Complexes –

Photochemical and Biomedical Applications (pp. 117–138), Wiley, Weinheim, 2018; (*d*) D. F. Azar, H. Audi, S. Farhat, M. El-Sibai, R. J. Abi-Habib and R. S. Khnayzer, *Dalton Trans.*, 2017, **46**, 11529–11532; (*e*) H. Chan, J. B. Ghrayche, J. Wei and A. K. Renfrew, *Eur. J. Inorg. Chem.*, 2017, 1679–1686; (*f*) M. H. Kaulage, B. Maji, S. Pasadi, S. Bhattacharya and K. Muniyappa, *Eur. J. Med. Chem.*, 2017, **139**, 1016–1029; (*g*) W. Li, Q Xie, L. Lai, Z. Mo, X. Peng, E. Leng, D. Zhang, H Sun, Y. Li, W. Mei and S. Gao, *Photodiagn. Photodyn. Ther.*, 2017, **18**, 83–94; (*h*) D. Tudor, I. Nenu, G. A. Filip, D. Olteanu, M. Cenariu, F. Tabaran, R. M. Ion, L. Gligor and I. Baldea, *PLoS ONE*, 2017, **12**, e0173241, doi:10.1371/journal.pone.0173241; (*i*) M. Durmus and V. Ahsen, *J. Inorg. Biochem.*, 2010, **104**, 297–309.

19 (*a*) T. Maisch, *Mini-Rev. Med. Chem.*, 2009, **9**, 974−983; (*b*) G. Jori and S. B. Brown, *Photochem. Photobiol. Sci.*, 2004, **3**, 403–405; *(c)* M. Kielmann, C. Prior and M. O. Senge, *New J. Chem.*, 2018, **42**, 7529–7550.

20 H. F. Chambers and F. R. DeLeo, *Nat. Rev. Microbiol.*, 2009, **7**, 629−641.

21 M. A. Bennett and A. K. Smith, *J. Chem. Soc., Dalton Trans.*, 1974, 233–241.

22 G. Li, A. Yella, D. G. Brown, S. I. Gorelsky, M. K. Nazeeruddin, M. Grätzel, C. P. Berlinguette and M. Shatruk, *Inorg. Chem.*, 2014, **53**, 5417–5419.

23 *(a)* H. Hope, *Prog. Inorg. Chem*., 1994, **41**, 1–19; *(b)* M. O. Senge, *Z. Naturforsch.*, 2000, **55b**, 336–344.

24 *(a)* SAINT, version 8.37a, Bruker AXS, Inc.; Madison, WI, 2013; (b) SADABS, version 2016/2, Bruker AXS, Inc.; Madison, WI, 2014; (c) APEX3, version 2016.9-0, Bruker AXS, Inc.; Madison, WI, 2016.

25 *(a)* O. V. Dolomanov, L. J. Bourhis, R. J. Gildea, J. A. K. Howard, and H. Puschmann, *J. Appl. Cryst*., 2009, **42**, 339–341; *(b)* G. M. Sheldrick, *Acta Cryst*., 2015, **A71**, 3–8.

26. Examples for other dipyrrinato ruthenium complexes: *(a)* G. Li, K. Hu, K. C. D. Robson, S. I. Gorelsky, G. J. Meyer, C. P. Berlinguette and M. Shatruk, *Chem. Eur. J.,* 2015, **21**, 2173–2181 (*b*) G. Li, L. Ray, E. N. Glass, K. Kovnir, A. Khoroshutin, S. I. Gorelsky and M. Shatruk, *Inorg. Chem.*, 2012, **51**, 1614–1624; *(c)* G. Li, P. G. Bomben, K. C. D. Robson, S. I. Gorelsky, C. P. Berlinguette and M. Shatruk, *Chem. Commun.,* 2012, **48**, 8790–8792; (*d*) M. Yadav, A. Kumar Singh, B. Maiti and D. Shankar Pandey, *Inorg. Chem.*, 2009, **48**, 7593–7603;

X1 (a) S. R. Halper, L. Do, J. R. Stork and S. M. Cohen, *J. Am. Chem. Soc.,* 2006, **128**, 15255–15268; (b) S. G. Telfer and J. D. Wuest, *Cryst. Growth Des.,* 2009, **9**, 1923–1931.